J. Mater. Environ. Sci. 7 (6) (2016) 2051-2068 *Moafi et al.*
ISSN : 2028-2508
CODEN: JMESCN

Ag_2O/Sawdust nanocomposite as an efficient adsorbent for removal of hexavalent chromium ions from aqueous solutions

H. F. Moafi, R. Ansari*, F. Ostovar
Department of Chemistry, Faculty of Science, University of Guilan, P.O.Box 1914, Rasht, Iran

Received 04 Jan 2015, Revised 27 Apr 2016, Accepted 28 Apr 2016
**Corresponding author. E-mail: Ransari271@guilan.ac.ir ; Phone: +9801333367262; Fax: +9801333367262*

Abstract
Ag_2O/sawdust nanocomposite (Ag_2O/SD NC) as adsorbent of Cr(VI) was prepared by precipitation method. The as-prepared sample was characterized by various techniques such as X-ray diffraction (XRD), scanning electron microscopy (SEM) and Fourier transform infrared spectroscopy (FT-IR). The SEM micrographs show formation of Ag_2O nanoparticles within 50–60 nm in size which have been homogeneously dispersed on the sawdust surface. The as-prepared Ag_2O/SD NC were used to remove Cr(VI) from aqueous solutions. To determine the optimal conditions for adsorption, the effect of important parameters such as pH, contact time, initial concentration of Cr(VI), amount of adsorbent, temperature and ionic strength were investigated. It was found that the Ag_2O/SD NC showed a high Cr(VI) removal capacity of 20.75 mg/g at 25 ^oC. The experimental data were well described by the pseudo-second-order kinetics and Langmuir isotherm model. Thermodynamic studies for the adsorption system were calculated and suggested that the adsorption process is spontaneous and exothermic. Taking advantages of the high adsorption capacity, inexpensive adsorbent, fast removal and easy separation from treated water, the Ag_2O/SD NC can be used as an efficient for Cr(VI) removal from aqueous solution. The exhausted adsorbent can be regenerated by simple alkaline treatment with high efficiency.

Keywords: Adsorption, Ag_2O/Sawdust nanocomposite, Cr(VI) Removal, Langmuir isotherm

1. Introduction
In the last years, environment contaminations by heavy metals such as chromium, mercury and copper has gained much attention due to the important impact on public health. Chromium is one of the most toxic pollutants generated by the electroplating, photography, leather tanning, metal finishing, dye and textile industries [1, 2]. In aqueous solutions chromium is commonly found in two stable oxidation states such as trivalent Cr(III) and hexavalent Cr(VI). Trivalent chromium is considered as an essential micronutrient for human, plant and animal metabolism and much less toxic than Cr(VI). While Cr(VI) is extremely toxic and carcinogenic to living organism [2, 3, 4]. Due to its high toxicity and bioaccumulation as well as its high mobility in the environment, the removal of Cr(VI) from contaminated aqueous solution is of great importance.
Developed and potential technologies such as coagulation [5, 6], electrochemical reduction [7], ion exchange [8, 9], membrane separation [10, 11], adsorption [12-16] have been used for the removal of Cr(VI). Compared to other methods, adsorption is proved to be an effective and convenient method due to its low initial cost, easy operation, flexibility in design, and insensitivity to biological materials in aqueous environment [3, 4]. Several kinds of materials have been used as adsorbent for removal of heavy metal ions, such as active carbon [17-19], oxide nanoparticles [20, 21], nanocomposites [22-24] and agriculture waste [25, 26], inorganic materials [27, 28], etc. These adsorbents showed good performance for the removal of Cr(VI) from aqueous solutions. Despite these advantages, many adsorbents suffer from some drawbacks such as low adsorption efficiency, impurity, high cost and slow kinetics. An ideal adsorbent should have a suitable particle size, accessible pores, large surface areas, and high environmental stability [4]. Therefore, recent advances in nanotechnology focuses

on the fabrication of nano-sized adsorbents with enhanced adsorption capacity and rapid sorption rate for the removal of contaminants. This could be due to the large surface area and highly active surface sites of the nanoadsorbents [3].
Today, alternative adsorbents derived from renewable resources or less expensive natural materials have attracted much interest for removal of pollutants from wastewaters. Sawdust as a waste material is one of the most attractive biomaterials used for removing of heavy metals and organic pollutants from aqueous media and the capability of sawdust as treated and untreated has been studied to remove pollutants from aqueous solutions [29-33].
In this work, a facile method was developed to produce an Ag_2O/sawdust nanocomposite. The adsorption properties of the nanocomposite toward Cr(VI) in aqueous solution were investigated. To determine the optimal conditions for absorption, the effect of important parameters such as pH, contact time, initial concentration of Cr(VI), adsorbent dose, and temperature were studied. The Ag_2O/Sawdust nanocomposite is found to possess unique capability such as easy separation, economical, cheap and commercially available adsorbent for the removal of Cr(VI) from aqueous solution.

2. Materials and methods

2.1. *Material*
All chemicals used were of analytical grade (AR) and were prepared in distilled water. Sawdust samples (SD) from dicer were obtained from a local carpentry workshop. Silver nitrate ($AgNO_3$), sodium hydroxide (NaOH), Potassium dichromate ($K_2Cr_2O_7$), 1, 5-di-phenylcarbazide was obtained from Merck.

2.2. *Instrumentation*
A magnetic stirrer, analytical scale and pH meter (model 827, Metrohm) with a combined double junction glass electrode, calibrated against two standard buffer solutions at pH 4.0 and 7.0 were used in experiments. The pH adjustments were made using dilute NaOH and HCl solutions. A single beam Perkin-Elmer UV-Vis spectrophotometer with a 1cm cell was used for measuring all the absorption data. Cr(VI) concentration was measured by UV-Visible Spectrophotometer (TU-1800PC Beijing) at 540 nm wavelength by 1,5 diphenyl carbazide method [34].

2.3. *Chemical synthesis*
Ag_2O/sawdust nanocomposite (Ag_2O/SD NC) was chemically prepared by the co-precipitation method. For this purpose, 5.0 g sawdust was poured into 50 mL of 0.20 M $AgNO_3$ and then 50 mL of a 0.40 M sodium hydroxide (NaOH) aqueous solution was added drop wise, while the solution was constantly stirred with a magnetic stirrer, until the solution had the consistency of a brown-black colloidal suspension. The solution was kept at 60 °C for 2 h to ensure complete reaction. After the heating and stirring for 2 h, the product was separated by filtration and washed with ethanol several times, and then dried at 80 °C. The reaction of silver nitrate with sodium hydroxide produces silver hydroxide via the following mechanism [35]:

$$AgNO_3 + NaOH \rightarrow AgOH\ (s) + NaNO_3$$

The intermediate AgOH is thermodynamically unstable, and upon mild heat treatment is converted into Ag_2O through the following dehydration process:

$$2AgOH(s) \rightarrow Ag_2O\ (s) + H_2O$$

2.4. *Preparation of Cr(VI) solution*
Chromium solutions were prepared by dissolving potassium dichromate in distilled water. For this purpose, 0.535 g potassium dichromate was dissolved to deionized water in a 1000 mL volumetric flask (stock solution of Cr(VI) with concentration of 200 mg/L).
2.5. Characterization of adsorbent
X-ray powder diffraction (XRD) patterns were obtained on a Philips PW1840 diffractometer at a voltage of 40 kV and a current of 100 mA with Cu Ka radiation (λ = 1.54056 Å). The surface morphology of Ag_2O/SD NC was examined using Scanning electron microscopy ((SEM) with unique thermo-emission electron source by a tungsten film, Germany and UK co-production model LEO 1430VP) at an accelerating voltage of 15.0 kV. The infrared spectra (400-4000 cm^{-1}) of samples were recorded on an alpha FT-IR (2011 Bruker Optic GmbH) instrument.

2.6. *Adsorption batch study*

The adsorption experiments of Cr(VI) from solutions by Ag_2O/SD NC was investigated in batch mode under various operational conditions. The Cr(VI) solutions for experiments with appropriate concentrations were prepared by diluting the stock solution (200 mg/L). The pH of the Cr(VI) solution was adjusted either by using either 0.10–0.01 M HCl or 0.10–0.01 M NaOH solutions and was varied within the range of 2–10. Various parameters such as pH (2-10), contact time (1 to 60 min), the initial concentration of Cr(VI) (15.0–200.0 mg/L), adsorbent dose (0.025-0.200 g), and temperature were studied. For the influence of parameters in each experiment, Cr(VI) solution with certain pH and the amount absorbent at 25^{o}C on shaker with 150 rpm speed were mixed. The volume of Cr(VI) solution was 25 mL with initial concentration 50 mg/L and the amount of adsorbent was 0.10 g. After shaking at a certain time, the solution was separated from the adsorbent by filtration. Measurement of unadsorbed Cr(VI) ion was carried out according to standard method by Gilcreas et al [36]. This method consists of measuring the absorbance at 540 nm of filtrate after adsorption and addition of a small amount of 1,5-diphenyl carbazide solution. This reagent makes a highly colored violet complex with Cr(VI) in 0.10 to 0.20 M H_2SO_4 [37].

The Cr(VI) removal efficiency was determined using the following equation:

$$\text{Removal } (\%)=C_0\text{-}C_e/C_0 \times 100 \quad (1)$$

Where C_0 is the initial concentration (mg/L) of Cr(VI) and C_e is the equilibrium concentration (mg/L). The equilibrium adsorption capacity (q_e) was determined using the following equation:

$$q_e=(C_0\text{-}C_e)V/m \quad (2)$$

Where C_0 is the initial concentration of Cr(VI) in solution (mg/L), C_e is the equilibrium concentration (mg/L), q_e is the equilibrium adsorption capacity (mg/L), m is the mass of adsorbent (g), and V is the volume of solution (L). At optimum pH value, the effect of adsorbent dose on the removal of Cr(VI) was studied with 25 mL of 50 mg/L solution at 25 ºC. The mass of adsorbent was varied from 0.025 g to 0.200 g.

The kinetic adsorption performance was studied by contacting 0.10 mg of Ag_2O/Sawdust nanocomposite with Cr(VI) solutions of two initial concentration at 25 ^{o}C. The initial pH of the Cr(VI) solution is 2.00, and the solution was shaked in a thermostatic shaker bath during the process. Samples were taken out of the solution at different time, each time 10 mL. The adsorption capacity was calculated by the following equation [38]:

$$q_t=(C_0\text{-}C_t)V/m \quad (3)$$

Where q_t is the adsorption capacity at time t, C_0 is the initial concentration of Cr(VI) in solution (mg/L), C_t is the Cr(VI) concentration at time t (mg/L), m is the mass of adsorbent (g), and V is the volume of solution (L). Thermodynamic parameters such as ΔH^o, ΔS^o and ΔG^o were also evaluated from equilibrium data. In addition, the kinetics was also studied, and the adsorption isotherms were investigated by the Langmuir, Freundlich and Temkin models.

3. Results and discussion

3.1. *XRD Analysis*

The XRD patterns of untreated sawdust, Ag_2O/SD NC and silver oxide nanoparticle are shown in Figure 1. The XRD pattern of sawdust is presented in Figure 1a. In Figure 1a, the bulk of the X-ray signal originated from the sawdust substrate. Figure 1b shows the XRD pattern of Ag_2O-covered sawdust. The XRD results show that the as-deposited Ag_2O has a great amount of Ag crystalline grains. The reflections observed at 2θ= 37.90° (111), 43.90° (200) and 64.18° (220) are related to the face-centered cubic (fcc) structure of metallic silver particle with the (111) reflection intensified considerably, in the presence of sawdust [39, 40]. The observed decrease in reflection intensity of sawdust after treating with silver oxide can be due to the strong interactions between silver or silver oxide with functional groups on the surface of sawdust.

Figure 1c shows the XRD pattern of Ag_2O nanoparticles and confirms the synthesized material to be Ag_2O. The XRD pattern for the Ag_2O nanoparticles had the following planes: 111, 200, 220, 311, and the 222 which correspond to the reflections observed at 2θ= 32.94°, 38.22°, 55.12° and 65.70° in Ag_2O with cubic system [35, 40]. The diameter of the Ag particles coated on sawdust surface and Ag_2O particles was calculated using the Scherrer formula:

$$D= K\lambda/\beta\cos\theta \quad (4)$$

Where *D* is the average diameter of the crystals in angstroms, λ, the X- ray wavelength for a Cu target (1.54˚ A), *K*, the crystal form factor (K = 0.89, corresponding to a crystal with an unknown shape), θ, the Bragg angle in degree and β is the full width at half maximum (FWHM) of the highest diffraction peak in radian. The value of k depends on several factors, including the shape of crystal and the miller index of the reflection plane. The characteristic peak of the coated Ag particles with the (111) reflection at 2θ=37.90 (crystal plane distance d= 2.37˚ A) was used to calculate its crystal diameter, and we obtained *D* = 12 nm (Figure 1b). Correspondingly, the size of the silver oxide particles was calculated *D* = 33.35 nm from the reflecting peak at 2θ=32.94 (Figure 1c).

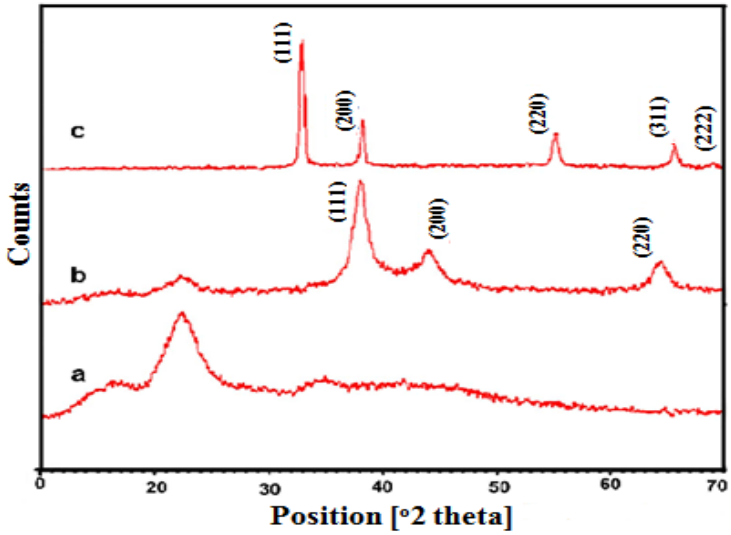

Figure 1: XRD patterns of: (a) pure sawdust, (b) Ag_2O-coated sawdust and (c) Ag_2O NPs.

3.2. *Morphology study*

In order to investigate the morphology of the obtained samples, surface morphology of the untreated, treated sawdust and Ag_2O nanoparticles was studied by scanning electron microscopy analysis (Figure 2 and Figure 3).

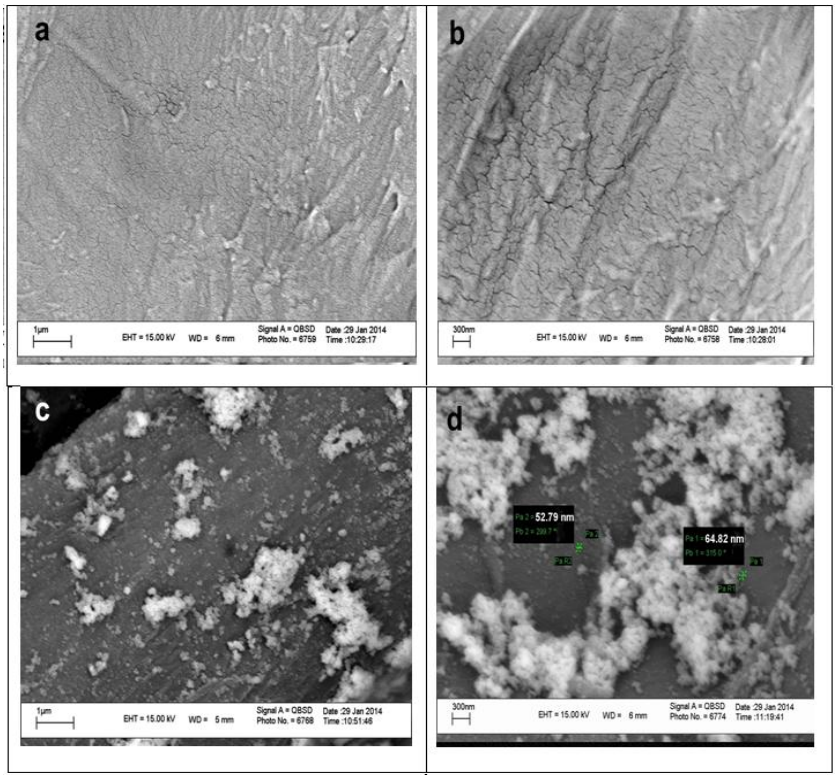

Figure 2: SEM images of: (a, b) pure sawdust and (c, d) Ag_2O-coated sawdust.

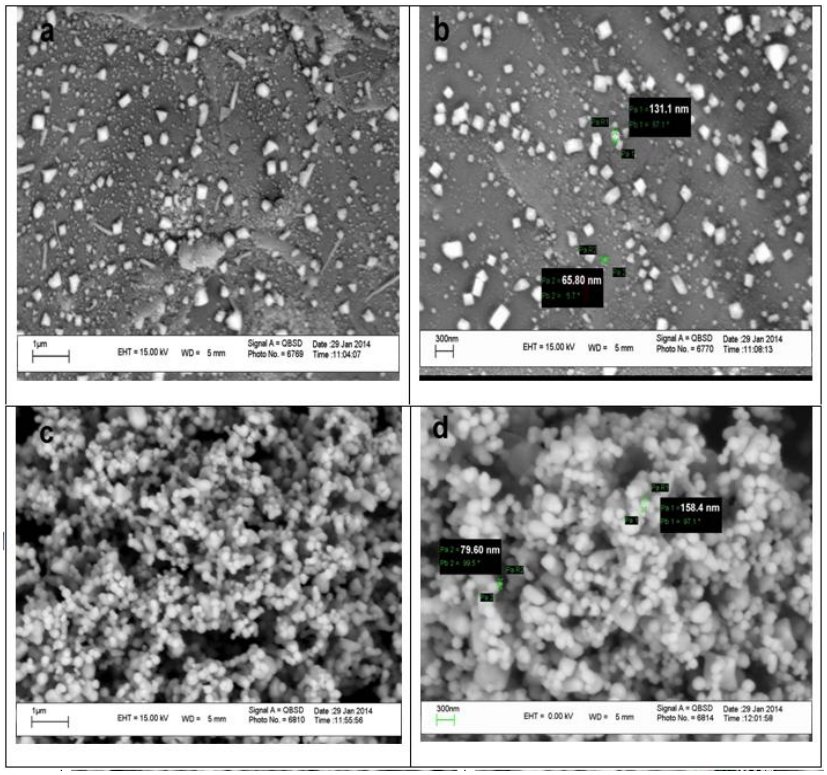

Figure 3: SEM images of: (a, b) Ag_2O-coated sawdust after adsorption of Cr(VI) and (c, d) Ag_2O particles.

Figures 2a and 2b show the surface of the pristine sawdust. The SEM micrographs show that the sawdust had a rough and porous surface. The comparisons between the SEM images of the treated and untreated sawdust clearly show that treated sawdust is covered by dispersed Ag and/or Ag_2O particles. It can be seen that the deposited nanoparticles were composed by agglomerates of fine particles with dimensions that are less than 100 nm and nanoparticles were uniformly distributed on the sawdust surface (Figure 2c and 2d). Figure 3a and 3b show the SEM image of treated sawdust after adsorption of Cr(VI). SEM images reveal that the most of Ag particles are irregularly shaped and relatively spherical with dimensions less than 100 nm. Its can clearly be seen the surfaces of adsorbent were covered by the fine particles and the bulk particles are separated. The SEM images of the powdered Ag_2O particles are shown in Figure 3c and 3d. The particles in this sample have relatively a sphere-like morphology. The image reveals that the most of them are agglomerates of irregularly shaped and relatively spherical with dimensions that are less than 100 nm.

3.3. *FT-IR spectroscopy study*

The FT-IR spectra of the untreated sawdust, Ag_2O, Ag_2O/SD NC before and after adsorption are shown in Figure 4. Figure 4a shows the FT-IR spectra of untreated sawdust. Sawdust has a fiber structure and its main component is cellulose, which has a straight chain structure and large molecule mass. The absorption peak at 3411 cm^{-1} indicates the hydroxyl groups and the absorption band at 2905 cm^{-1} is due to the contribution from C-H stretching. The band at 2359 cm^{-1} is assigned to stretching vibrations of N–H or C=O groups probably due to amines and ketones, 1647 cm^{-1} is an indication of COO, C=O, and can also indicate the bending vibration of adsorbed water, 1268 cm^{-1} is assigned to carboxylic acids vibration, 1058 cm^{-1} is stretching vibration of C–O–C and O–H of polysaccharides. The band at around 1428 cm^{-1} is assigned to symmetric COO– stretching motions and to the bending vibrations of aliphatic groups, whereas the peak at 1372 cm^{-1} refers to C-O stretching of cellulose in sawdust [41].

FT-IR spectrum of Ag_2O nanoparticles is presented in Figure 4b. It represents several bands at 3375, 1651, and 1385 cm^{-1}. The absorption peak at 3375 cm^{-1} indicates the hydroxyl groups, 1651 cm^{-1} is a bending vibration of adsorbed water and the absorption band at 1385 cm^{-1} could be assigned to CO_2 stretching vibration (carbon dioxide from atmosphere, perhaps due to the mesoporous nature of Ag_2O nanomaterials).

The Ag-O-Ag stretching vibration band could be appeared at around of 509 cm^{-1} which is covered due to the overspread of spectra in region 400-500 cm^{-1} [42].
Figure 4c shows the FT-IR spectra of Ag_2O/SD NC. FT-IR spectrum analysis confirms that the silver oxide nanoparticles are dispersed onto the sawdust. The intensity of some bands has decreased because of the presence of silver oxide nanoparticles onto the sawdust. The bands at 1647, 1428 and 1058 cm^{-1} were shifted to 1642, 1416, 1030 cm^{-1} respectively in the Ag_2O/SD nanocomposite and it proves the interaction of silver oxide nanoparticles with the different reaction sites of sawdust. FT-IR spectra of Ag_2O/SD NC after adsorption of Cr(VI) is shown in Figure 4d. Two new peaks were observed in FTIR spectra of Cr(VI)-loaded sorbents (807 and 900 cm^{-1}) attributed to Cr-O and Cr=O bonds of $HCrO_4^-$, which suggests that Cr(VI) was adsorbed on the surface of Ag_2O/SD NC [43, 44].
As shown in the Figures 4a, 4c and 4d, the some wave number shifts in the main peaks of sawdust compared with Ag_2O/SD NC, it might be concluded that some metal binding between sawdust and silver oxide taking place at the surface of the sawdust [15]. Formation of some metallic silver particles as confirmed by XRD, some oxidation reaction occurred on the surface of sawdust (as reductant). However, the adsorption mechanism could be considered as mixture of chemisorption and electrostatic interaction. Electrostatic interactions between silver based nanocomposite and Cr (VI) ions (mainly existed as $HCrO_4^-$ form at pH 2) seems to be the dominant reason for uptake of Cr(VI) ions by Ag_2O/SD NC.

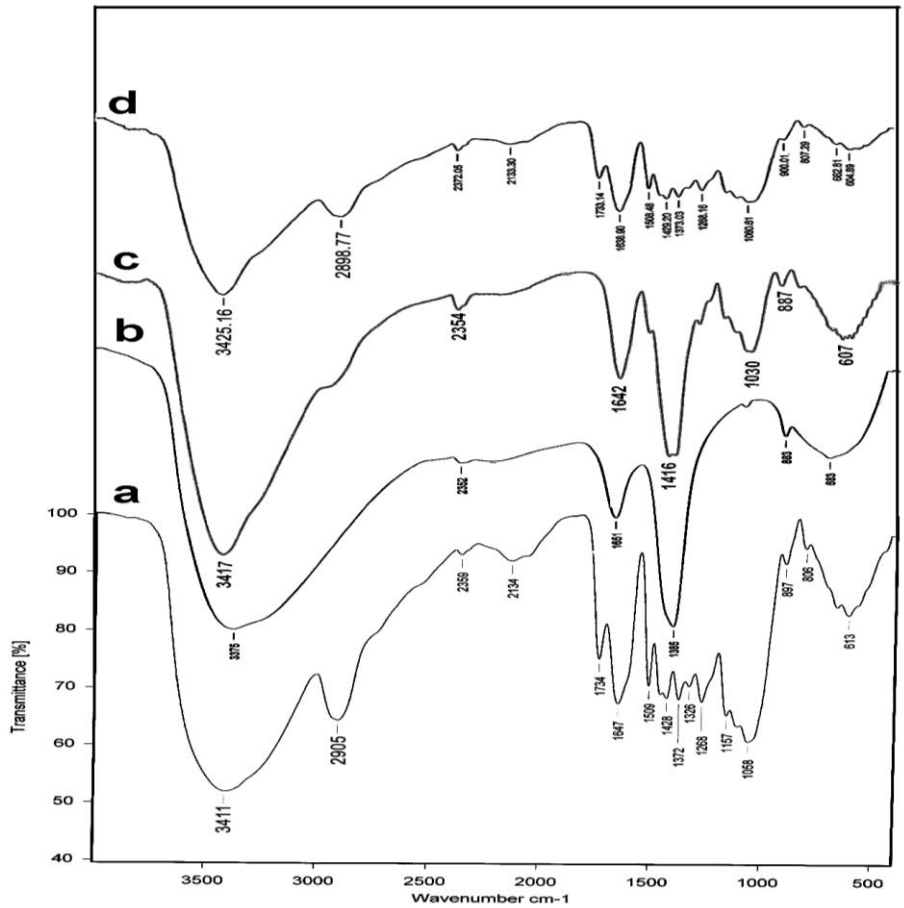

Figure 4: FT-IR of: (a) pure sawdust, (b) Ag_2O NPs (c) Ag_2O-coated sawdust and (d) Ag_2O/SD NC after adsorption of Cr(VI).

3.2. *Batch adsorption study*
3.2.1 *Effect of pH on Cr(VI) removal*
The initial solution pH is one of the most important environmental factors strongly influence on the adsorption of Cr(VI). The effect of pH was examined by varying the pH of the solution in the range 2.00–10.00 using 25 mL an initial concentration of 50.0 mg/L of Cr(VI) by aliquots of adsorbents (0.10 g) at 298 K and is

illustrated in Figure 5. It is found that the adsorption capacity is highly dependent on the pH of the solution. Cr(VI) removal is improved with decreasing pH from 10.0 to 2.0 for all adsorbents (sawdust, Ag_2O and Ag_2O/SD NC). As a result, the optimum pH for Cr(VI) adsorption was found as 2.0 and the other adsorption experiments were performed at this pH. According to the literature [3], the predominant Cr(VI) species are monovalent bichromate ($HCrO_4^-$) and divalent dichromate ($Cr_2O_7^{2-}$) when the pH is in the range of 2.0–6.0, while the dominant species is chromate (CrO_4^{2-}) when the pH is above 6.0. As shown in Figure 5, when the pH of the initial solution changed from 10.0 to 2.0, the adsorption efficiency increased from 45.5% to about 99%. Removal of $HCrO_4^-$ anions using Ag_2O/SD NC increased at pH 2 owing to the formation of positive charges on the adsorbent surface (due to high concentration of H^+ at acidic conditions) and electrostatic interactions between adsorbent and adsorbate. The reason for the decrease of adsorption efficiency at alkaline pH values is due to the repulsive interactions between the negatively charged adsorbent surface (due to high concentration of OH^- at alkaline conditions) and CrO_4^{2-} anions[2, 3].

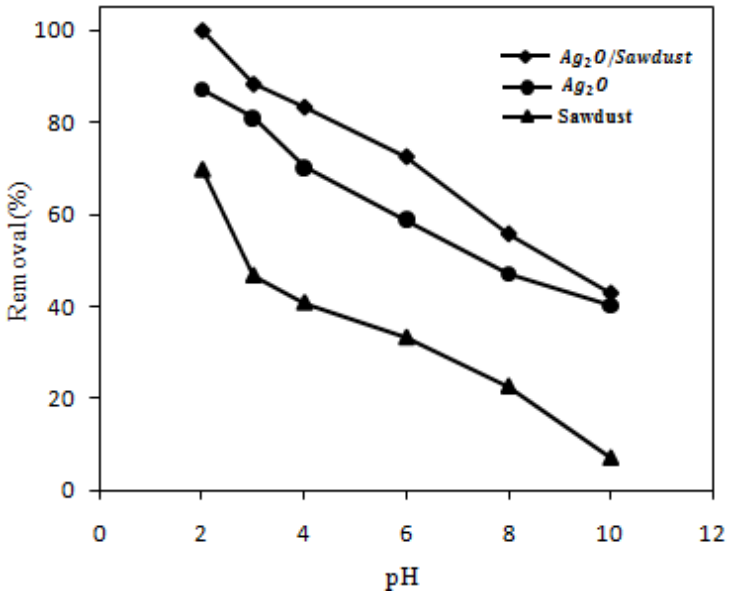

Figure 5: The effect of initial pH of solution on the percentage removal of Cr(VI) from solution on sawdust, Ag_2O and Ag_2O/SD NC (initial concentration of Cr(VI) 50 mg/L, adsorbent dose 0.1 g, temperature 298 K, and contact time 30 min).

3.2.2 *Effect of contact time*

The Effect of contact time on adsorption of Cr(VI) ions was studied by shaking mixture of 0.10 g adsorbent (Ag_2O/SD NC) with 50 mL of the aqueous solutions of Cr(VI) ions with initial concentrations of 50.0 and 75.0 mg/L at acidic pH (pH= 2). The effect of contact time on the percentage removal of Cr(VI) ion is presented in Figure 6. The data obtained from the adsorption of Cr(VI) ion on the Ag_2O/SD NC showed that the adsorption increases with an increasing contact time. For a concentration less than 50.0 mg/L Cr(VI) the maximum adsorption was reached in a short period of time and the composite adsorbed approximately 100% of the metal ion. The result indicates that a fast adsorption process of Cr(VI) occurred during the first few minutes. The plot reveals that the rate of percentage removal of Cr(VI) ion is initially high which is probably due to the availability of larger surface area of the Ag_2O/SD NC for the adsorption of Cr(VI) ions. The maximum percentage removal of Cr(VI) ion was attained after 30 min of stirring time. The adsorption did not changed much with further increase in contact time. Therefore, the contact time of 30 min was sufficient to achieve equilibrium for Cr(VI) ion.

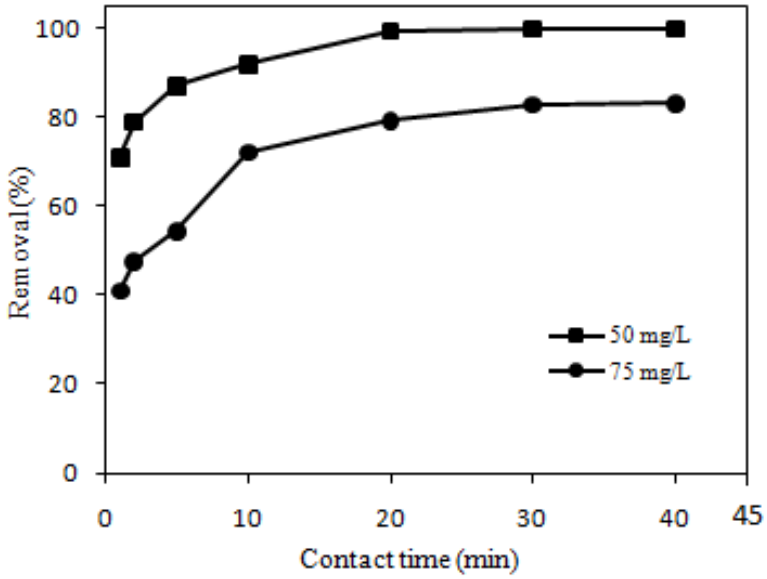

Figure 6: The Effect of time contact on the percentage removal of Cr(VI) on Ag_2O/SD NC (pH 2, initial concentration of Cr(VI) 50 mg/L, adsorbent dose 0.1 g, and temperature 298 K).

3.2.3. *Effect of initial concentration of Cr(VI) on the removal*

The initial metal ion concentration is another important variable that can affect the adsorption process. The rate of adsorption or adsorption capacity is a function of initial metal ion concentration. The effect of chromium concentration on the adsorption was studied under optimized pH. For this investigation, 0.10 g of Ag_2O/SD NC were treated with 50 mL of Cr(VI) ion solution with different initial concentrations. Concentrations of Cr(VI) varied from 15.0 to 200.0 mg/L. The effect of initial Cr(VI) concentration on removal efficiency of the adsorbent is presented in Figure 7. It can be seen that with increasing initial concentration of chromium removal efficiency decreases. So, with increasing of initial concentration of chromium from 15.0 to 200.0 mg/L, the absorption rate is reduced from 100.00% to 55.57%. Decrease in adsorption percentage at higher concentrations might be due to the relatively smaller numbers of active sites available at higher chromium concentrations. On the other hand, at higher concentrations, the available sites of adsorption become fewer, and hence the percentage removal of metal ions depends upon the initial concentration [41].

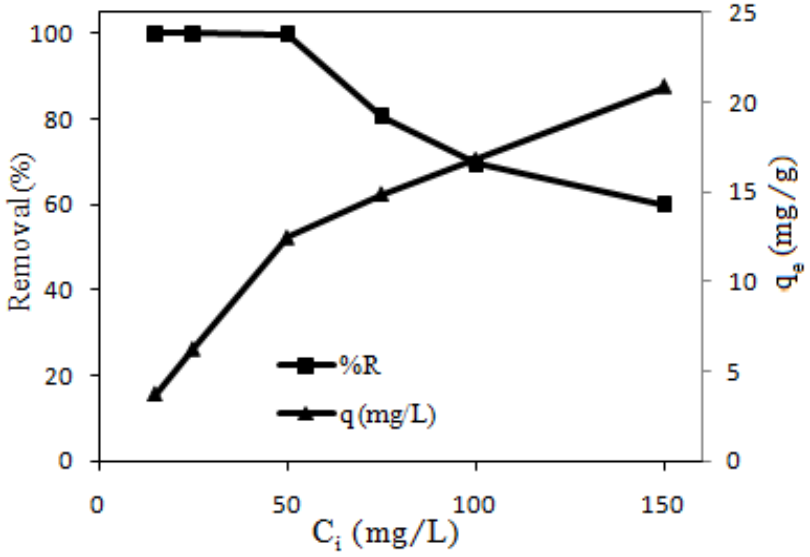

Figure 7: The effect of initial concentration of Cr(VI) on the percentage removal of Cr(VI) ion from solution on Ag_2O/SD NC (pH 2.0, adsorbent dose 0.1 g, temperature 298 K, and contact time 30 min).

3.2.4 *Effect of the dosage of Ag_2O/SD NC*

Adsorbent dosage is an important parameter because it determines the capacity of an adsorbent for adsorption of an adsorbate. In this experiments, Cr(VI) solution (50 mL, 50.0 mg/L) was treated with various amounts of the Ag_2O/SD NC (from 0.025 to 0.200 g) at pH 2.0 and room temperature for 30 min. Figure 8 shows the effect of adsorbent dosage on the removal efficiency (% removal) of Cr(VI) from aqueous solution. The results indicated that the percentage removal of Cr(VI) rapidly increased (from 59.0% to 100.0%) with the increase of dosage (from 0.025 to 0.200 g). This is due to an increase in the surface area and availability of more active sites of the adsorbent for uptake of Cr(VI) ions [3]. After optimum dosage (0.100 g), the removal efficiency remains unchanged with increase in adsorbent dosage. Further increase in adsorbent dosage (>0.10 g) did not create significant improvement in Cr(VI) removal efficiency. This seems to be due to the binding of almost all ions to the adsorbent and the establishment of equilibrium. It has been reported that there are many factors which can contribute to adsorbent dosage effect on efficiency of adsorption. The most important factor is that adsorption sites remain unsaturated during adsorption process. As the adsorbent dosage is increased, the adsorption increased slightly resulting from the lower adsorptive capacity utilization of the adsorbent. The other reason may be the aggregation/agglomeration of adsorbent particles at higher dosages, which would lead to a decrease in the surface area and an increase in the diffusion path length. The particle interaction at higher adsorbent dosage may also help to desorbs some of the loosely bound metal ions from the sorbent surface [45].

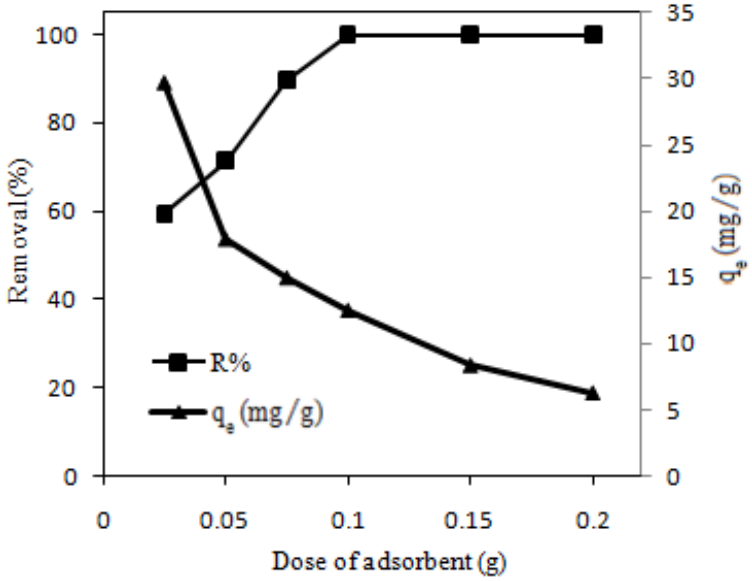

Figure 8: The effect of adsorbent dosage on the percentage removal of Cr(VI) ion from solution on Ag_2O/SD NC (pH 2.0, metal concentration 50 mg/L, temperature 298 K, and contact time 30 min).

3.3. *Equilibrium isotherms studies*

Adsorption isotherms are basic requirements for designing of an adsorption system. Isotherm expresses the relation between the amounts of adsorbate removed from the aqueous solution by unit of mass of sorbent at constant temperature [46, 47]. The parameters of adsorption isotherms provide useful insight into both sorption mechanism and surface properties. Therefore it is important to create the most suitable correlation of equilibrium curves in order to optimize the conditions for the design of adsorption systems [46, 47]. To quantify the adsorption capacity of Ag_2O/SD NC for the removal of Cr(VI) from aqueous solution, the Langmuir, Freundlich and Temkin isotherm models were used at various temperatures.

3.3.1. Langmuir and Freundlich isotherms

The Langmuir model assumes that the adsorption of metal ions occurs on a homogeneous surface by monolayer adsorption, and no interaction happens between sorbent species [3]. The Freundlich model assumes physicochemical adsorption on heterogeneous surfaces. The linearized Langmuir (Eq. (5)) and Freundlich (Eq. (6)) models are expressed as follows:

$$C_e/q_e = 1/q_m.b + C_e/q_m \quad (5)$$

$$Ln\ q_e = \ln k_F + 1/n\ (\ln C_e) \quad (6)$$

Where q_e is the amount of adsorbate adsorbed per mass of adsorbent at equilibrium (mg/g), C_e is the equilibrium concentration of adsorbate in aqueous solution (mg/L), q_m is the maximum adsorption capacity (mg/g) of the Ag_2O/SD NC, b is the free energy of adsorption (L/mg), k_F and n are the Freundlich isotherm parameters related to adsorption capacity (mg/g) and intensity of adsorption, respectively. The linearized plots of Langmuir, Freundlich and Temkin isotherms are shown in Figures 9a–9c, respectively. From the linear equation of the plots, the calculated parameters of the isotherms are presented in Table 1. The monolayer adsorption capacity (q_m) was obtained as 20.75 mg/g for Ag_2O/SD NC which is considerably higher than SD and Ag_2O nanoparticles. Based on the higher values of correlation coefficients (R^2) for Langmuir model (R=0.9905) compared to the Freundlich model (R=0.8806), adsorption data seems to be described by the Langmuir model more favourably. On the other hands, the Langmuir model is more suitable than the Freundlich model for describing the adsorption process, indicating that the adsorption of Cr(VI) on the Ag_2O/SD NC is homogenous.

The favorability (the essential features of the Langmuir isotherm) of the adsorption process was also represented by a dimensionless constant separation factor R_L (R_L, also called equilibrium parameter), which is defined by the Eq. (7) [46]:

$$R_L=1/(1+bC_0) \quad (7)$$

Where C_0 is the initial concentration (mg/L) and b is the Langmuir constant (L/mg). The value of R_L represents the adsorption process to be unfavorable when $R_L>1$, linear when $R_L=1$, favourable when $R_L<1$ and irreversible when $R_L=0$ [3]. For this studied, R_L values fall between 0 and 1 (Table 1) confirming the favourable nature of adsorption of Cr(VI) by the Ag_2O/SD NC.

3.3.2. *Temkin isotherm model*

The Temkin isotherm model unlike the Langmuir and Freundlich isotherms contains a factor that explicitly takes into account the interactions between adsorbents and metal ions to be adsorbed and is based on the assumption that the free energy of sorption is a function of the surface coverage [3, 46]. On the other hand, the Temkin isotherm assumes that the heat of adsorption in the layer decreases linearly with coverage due to the interactions between adsorbate and adsorbate. Also, this model assumes that adsorption process is characterized by a uniform distribution of binding energies, up to some maximum binding energy [48]. Temkin isotherm is represented by following equation:

$$q_e=(RT/b_T)\ln(k_TC_e) \quad (8)$$

Equation (8) can be expressed in its linear form as:

$$q_e=B\ \ln k_T + B\ \ln C_e \quad (9)$$

Where k_T is the equilibrium binding constant corresponding to the maximum binding energy (L/g), b_T is the Temkin constant related to the heat of adsorption (KJ/mol), R is the universal gas constant (8.314 J/mol.K) and T is the absolute temperature (K) [3]. The adsorption data can be analyzed according to equation (9). A plot of q_e versus $\ln C_e$ enables the determination of the isotherm constants K_T and B. This isotherm is plotted in Figure 9c for Cr (VI) adsorption on Ag_2O/SD NC and the values of the related parameters of the used adsorbents are also given in Table 1.

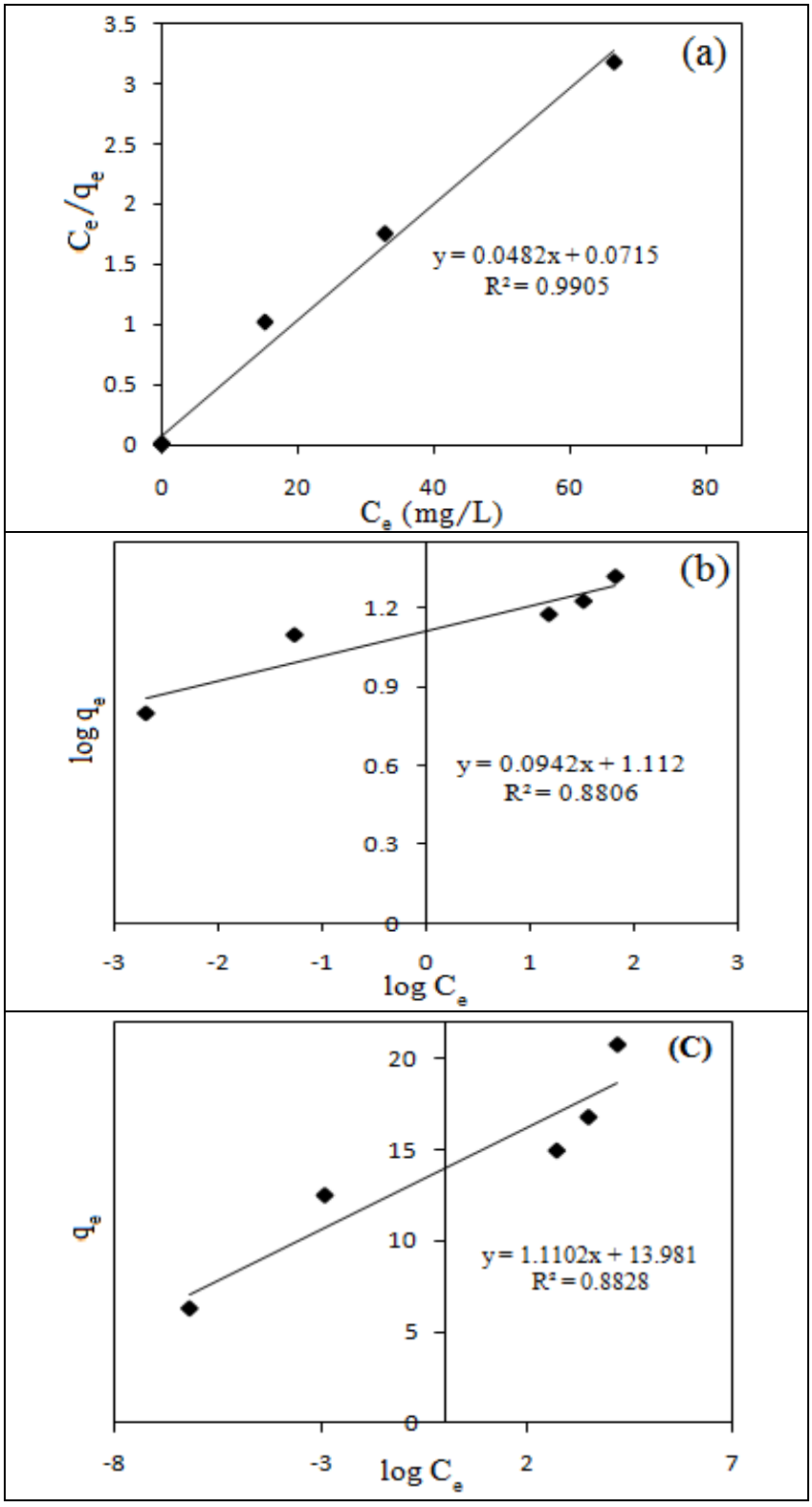

Figure 9: The linear plot of adsorption equilibrium data. (a) Langmuir isotherm, (b) Freundlich isotherm and (c) Temkin isotherm (Conditions: pH 2.0, adsorbent dose 0.10 g, temperature 298 K, and contact time 30 min).

Table 1: The Freundlich, Langmuir and Temkin equilibrium adsorption isotherm models for adsorption of Cr(VI) on the used adsorbents

Lungmuir constant				
Adsorbent	q_m (mg/g)	b (L/mg)	R^2	R_L
Ag_2O/SD NC	20.75	0.674	0.9905	0.015
Ag_2O NPs	12.77	0.546	0.9817	0.012
SD	6.67	0.078	0.9729	0.078
Freundlich constant				
Adsorbent	n	K_F (L/g)	R^2	
Ag_2O/SD NC	10.61	12.94	0.8806	
Ag_2O NPs	3.85	4.77	0.8833	
SD	3.06	1.37	0.8529	
Temkin constant				
Adsorbent	K_T (L/mg)	B	R^2	
Ag_2O/SD NC	2.53	1.11	0.8828	
Ag_2O NPs	11.34	2.03	0.9313	
SD	1.21	1.24	0.8700	

It was found that the correlation coefficient (R^2) for the Langmuir isotherm model was 0.9905, which was higher than that of Freundlich isotherm model (0.8806) and Temkin isotherm model (0.8828). This suggests that the Langmuir model provided a more consistent fit to the data compared with the Freundlich and also Temkin models. In sawdust, various functional surface groups (e.g. phenolic –OH, aliphatic C–H and carboxylic groups) can be responsible for Cr(VI) removal. Both sawdust and silver oxide are capable to uptake Cr(VI) ions as indicated in Table 1. However, the nanocomposite was found to be more effective due to the synergistic effect.

3.4. *Adsorption kinetics*

Adsorption kinetic study provides valuable information on the reaction pathways and the mechanism of adsorption process [37]. The mechanism of adsorption depends on the physical and chemical characteristics of the adsorbents. The kinetics of adsorption explains the rate of uptake of chromium ions onto the Ag_2O/SD NC and this rate controls the equilibrium time. In order to investigate the kinetic mechanism of Cr(VI) sorption onto the Ag_2O/SD NC, kinetic models including pseudo-first order (Eq. 10) and pseudo-second order (Eq. 11) were examined

$$\log (q_e - q_t) = \log q_e - k_1 t/2.303 \quad (10)$$

$$t/q_t = 1/k_2 q_e^2 + t/q_e \quad (11)$$

Where q_e (mg/g) and q_t (mg/g) are amount of Cr(VI) adsorbed at equilibrium and at time t (min), k_1 (1/min) and k_2 (g/min.mg) are the pseudo-first order and pseudo-second order adsorption rate constant, respectively [3]. The values of k_1 and q_e for the pseudo-first order model were determined from the slope and intercept of the plot of log (q_e-q_t) against t as indicated in Figure 10a. Values of k_2 and q_e for the pseudo-second order model were calculated from the slope ($1/q_e$) and intercept ($1/K_2 q_e^2$) of the linear plot of t/q_t versus t as indicated in Figure 10b. The conformity between experimental data and the model predicted values was expressed by the correlation coefficient (R^2). The resulting kinetics data calculated for the three adsorbents are also summarized in Table 2.

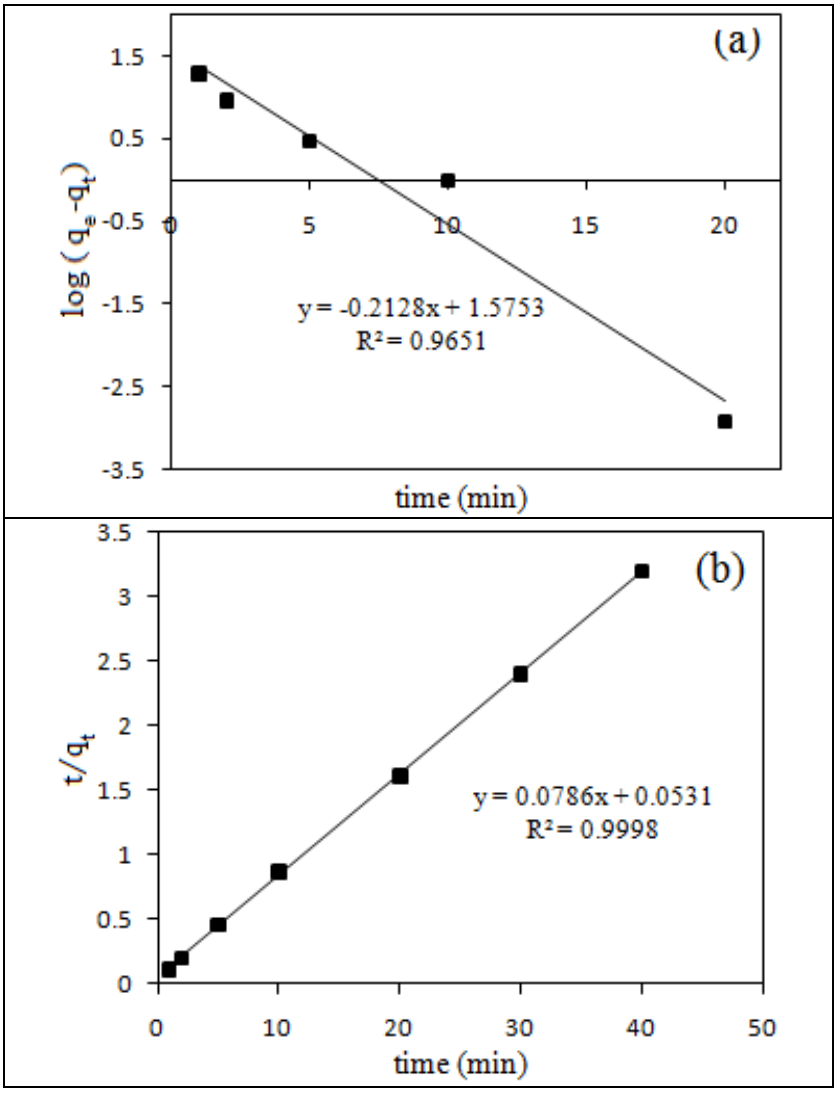

Figure 10: Cr(VI) adsorption on Ag_2O/SD NC. (a) Pseudo-first order and (b) Pseudo-second order kinetics

Table 2: Parameters obtained from the kinetics models for the used adsorbents

Adsorbent	Pseudo-first-order model				Pseudo-second-order model		
	$q_{e,exp}$ (mg/g)	K_1 (1/min)	$q_{e,cal}$ (mg/g)	R^2	K_2 (g/mg.min)	$q_{e,cal}$ (mg/g)	R^2
Ag_2O/SD NC	12.43	0.490	4.83	0.9651	0.116	12.72	0.9998
Ag_2O NPs	10.89	0.076	2.45	0.9603	0.104	11.17	0.9989
SD	5.37	0.107	2.975	0.9636	0.072	5.81	0.9982

It can be seen that values of correlation coefficients for pseudo-second-order model are greater than those of pseudo-first-order model. Moreover, the calculated value of q_e for pseudo-second-order model is much closer to the experimental values of q_e (Table 2). Therefore, it could be concluded that the sorption of Cr(VI) onto Ag_2O/SD NC follows the pseudo-second order kinetics model and Cr(VI) removal is mainly governed by chemical sorption. Based on the regression analysis and the closeness of the experimental adsorption capacity

($q_{e\ exp}$) to $q_{e\ cal}$ for the used adsorbents, chemisorptions and pseudo-second order kinetics model could be suggested.

3.8. *Thermodynamic investigations*

The thermodynamic parameters associated with the adsorption process, namely, standard Gibbs free energy change (ΔGº), entropy change (ΔSº) and enthalpy change (ΔHº) were calculated using the following equations:

$$\Delta G^{o} = -RT \ln K_C \quad (12)$$

$$\ln K_c = \Delta S^{o}/R - \Delta H^{o}/RT \quad (13)$$

Where R (J/mol/K) is the ideal gas constant, T (K) is the absolute temperature and Kc (L/mol) is the thermodynamic equilibrium constant [3]. The thermodynamic parameters of adsorption of Cr(VI) onto Ag_2O/SD NC calculated from the slope and intercept of the linear plot of $\ln K_c$ versus 1/T is represented in Figure 11. The thermodynamic parameters obtained for the three adsorbents are summarized in Table 3.

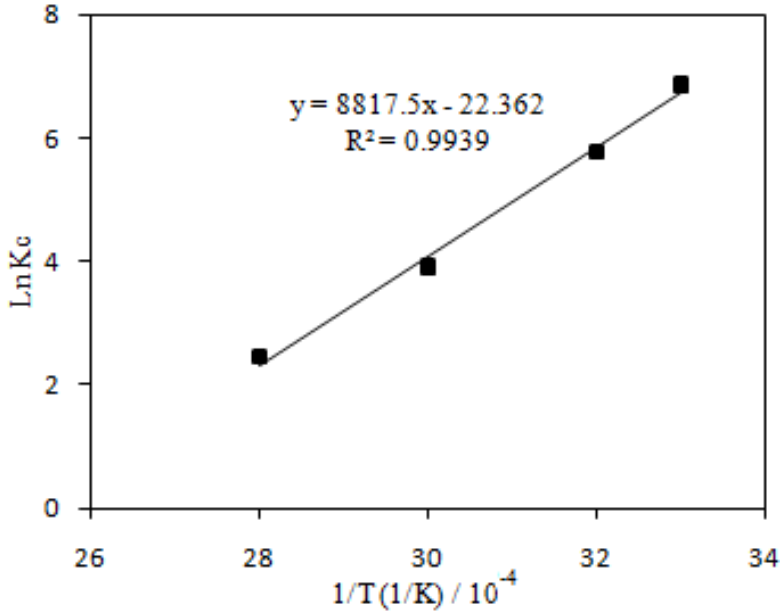

Figure 11: The plot of ln K_c versus 1/T for Cr(VI) adsorption on Ag_2O/SD NC.

Table 3: Thermodynamic parameters for Cr(VI) uptake for the used adsorbents

Adsorbent	Temperatures (K)	K_c	ΔG^{o} (KJ/mol)	ΔH^{o} (KJ/mol)	ΔS^{o} (J/mol.K)
Ag_2O/SD		960.5	-17.02	-73.31	-185.92
Ag_2O	298	6.78	-4.74	-0.983	-16.54
SD		0.754	0.69	-0.908	-32.50
Ag_2O/SD		323.7	-14.80		
Ag_2O	308	5.87	-4.53		
SD		0.646	1.13		
Ag_2O/SD		49.4	-10.66		
Ag_2O	328	4.92	-4.20		
SD		0.527	1.69		
Ag_2O/SD		11.6	-6.89		
Ag_2O	338	3.68	-3.55		
SD		0.431	2.29		

It is obvious that the negative values of free energy change in all the systems indicate the spontaneous nature of the process. On the other hand, with an increase in temperature negative values of change in Gibbs free energy (ΔG°) are obtained which reveal the spontaneity of the adsorption process. The negative values of standard enthalpy change suggest the exothermic nature of the adsorption process and the negative values of ΔS° indicate faster interaction during the forward reaction (sorption). As shown (Table 3) from the thermodynamic investigations, it can be concluded that Cr(VI) sorption onto Ag_2O/SD nanocomposite is more favourable.

3.9. Desorption studies

Since the adsorption of Cr(VI) ions onto Ag_2O/SD NC is pH-dependent and the lower pH is beneficial for the Cr(VI) adsorption, the desorption of Cr(VI) ions from the adsorbent can be achieved by increasing the system pH values. Therefore, for performing desorption studies the exhausted Ag_2O/SD NC was treated with 0.10 M NaOH and 5 wt% ammonia solution in order to regenerate the Ag_2O/SD NC. It was found that more than 95% of the pre-adsorbed Cr(VI) ions can be desorbed upon simple treatment of Ag_2O/SD particles with 0.01 M of NaOH solution. Desorption investigation showed that the introduced adsorbent in the current research can be used for Cr(VI) removal with high regeneration efficiency (>95%).

3.10. *Adsorption capacity of the prepared nanocomposite compared to some reported adsorbents*

The adsorption capacity of Ag_2O/SD NC for Cr(VI) ions removal was compared with some other reported adsorbents (Table 4). As shown, the adsorption capacity achieved in this work is higher than most of them. Therefore, it can be concluded that Ag_2O/SD NC is an effective adsorbent for Cr(VI) ions removal from aqueous solutions.

Table 4: Comparison of the adsorption capacities of Ag_2O/Sawdust NC with some reported adsorbents for Cr(VI) removal.

umber	Adsorbents	Adsorption capacity (mg/g)	Ref. No
1	Neem bark	19.60	[14]
2	Rice straw	12.172	[15]
3	Rice husk	11.398	[15]
4	Hyacinth roots	15.281	[15]
5	Neem leaves	15.954	[15]
6	Base extracted sawdust	10.10	[41]
7	Sawdust	5.50	[41]
8	Tartaric acid modified sawdust	10.72	[41]
9	Treated sawdust of Sal tree	9.55	[49]
10	Modified red pine sawdust	22.6	[50]
11	Coconut shell based activated carbon	20	[51]
12	Ag_2O/Sawdust	20.75	**This study**

Conclusions

Ag_2O/Sawdust nanocomposite was prepared as a good alternative biosorbent for removal of Cr(VI) from aqueous solution. The nanocomposite was used without any chemical treatment presenting biosorption capacities for efficient removal of Cr(VI). The performance of prepared nanocomposite for Cr(VI) removal from aqueous solution was investigated by batch adsorption experiments. The optimum pH for the maximum removal of Cr(VI) was found to be about 2.0. The adsorption and equilibrium data closely follows the Langmuir adsorption isotherm demonstrating that monolayer adsorption mechanism and chemisorptions process. The monolayer adsorption capacity (q_m) as estimated from the Langmuir isotherm is 20.75 mg/g. Kinetic data and correlation coefficients (R^2) confirm that sorption of Cr(VI) onto Ag_2O/Sawdust

nanocomposite follow the pseudo-second order kinetics model. The adsorption process is spontaneous nature and exothermic, which is confirmed by the evaluated thermo dynamical parameters. Its use can be interesting in the commercial and environmental viewpoint because of its low preparation cost, high sorption capacity and regeneration efficiency.

Acknowledgment-The authors appreciate the Research Department of university of Guilan for partially financial support of this work.

References

1. Vieira R.S., Lisa M., Oliveira M., Guibal E., Rodríguez-Castellón E., Beppu M.M., Copper, mercury and chromium adsorption on natural and crosslinked chitosan films: An XPS investigation of mechanism, *J. Colloid. Surf. A: Physicochem. Eng. Aspects*. 374 (2011) 108-114.
2. Wang J., Pan K., He Q., Cao B., Polyacrylonitrile/polypyrrole core/shell nanofiber mat for the removal of hexavalent chromium from aqueous solution, *J. Hazard. Mater*. 244-245 (2013) 121-129.
3. Bhaumik M., Maity A., Srinivasu V.V., Onyango M.S., Removal of hexavalent chromium from aqueous solution using polypyrrole-polyaniline nanofibers, *Chem Eng J*. 181-182 (2012) 323-333.
4. Lv X., Xu J., Jiang G., Tang J., Xu X., Highly active nanoscale zero-valent iron–Fe_3O_4 nanocomposites for the removal of chromium(VI) from aqueous solutions, *J. Colloid Interface Sci*. 369 (2012) 460-469.
5. Taa N., Benyahya M., Chaouch M., Using a bio-flocculent in the process of coagulation flocculation for optimizing the chromium removal from the polluted water, *J. Mater. Environ. Sci.* 7 (5) (2016) 1581-1588.
6. Xu H.Y., Yang Zh.H., Zeng G.M., Luo Y.L., Huang J., Wang L., Song P.P., Mo X., Investigation of pH evolution with Cr(VI) removal in electrocoagulation process: Proposing a real-time control strategy, *Chem. Eng. J*. 239 (2014) 132-140.
7. Liu Y., Yuan D., Yan J., Li Q., Ouyang T., Electrochemical removal of chromium from aqueous solutions using electrodes of stainless steel nets coated with single wall carbon nanotubes, *J. Hazard. Mater*. 186 (2011) 473-480.
8. Edebali S., Pehlivan E., Evaluation of Amberlite IRA96 and Dowex 1× 8 ion-exchange resins for the removal of Cr(VI) from aqueous solution, *Chem. Eng. J*. 161 (2010) 161-166.
9. Sardohan T., Kir E., Gulec A., Cengeloglu Y., Removal of Cr(III) and Cr(VI) through the plasma modified and unmodified ion-exchange membranes, *Sep. Purif. Technol*. 74 (2010) 14-20.
10. Gomes S., Cavaco S.A., Quina M.J., Gando-Ferreira L.M., Nanofiltration process for separating Cr(III) from acid solutions: experimental and modeling analysis, *Desalination*. 254 (2010) 80-89.
11. Goyal R.K., Jayakumar N.S., Hashim M.A., A comparative study of experimental optimization and response surface optimization of Cr removal by emulsion ionic liquid membrane, *J. Hazard. Mater*. 195 (2011) 383-390.
12. Prabhakaran S.K., Vijayaraghavan K., Balasubramanian R., Removal of Cr(VI) ions by spent tea and coffee dusts: reduction to Cr(III) and biosorption, Ind. *Eng. Chem. Res*. 48 (2009) 2113-2117.
13. Merabet S., Boukhalfa C., Chellat S., Boultif A., Characterization of chromium (III) removal from water by river bed sediments: Kinetic and Equilibrium studies, *J. Mater. Environ. Sci.* 7 (5) (2016) 1624-1632.
14. Bhattacharya A.K., Naiya T.K., Mandal S.N., Das S.K., Adsorption, kinetics and equilibrium studies on removal of Cr(VI) from aqueous solutions using different low-cost adsorbents, *Chem. Eng. J. 137 (2008) 529–541*.
15. Singha B., Das S.K., Biosorption of Cr(VI) ions from aqueous solutions: Kinetics, equilibrium, thermodynamics and desorption studies, *Colloids and Surfaces B: Biointerfaces 84 (2011) 221–232*.
16. Kouider M., Asmâa M., Lahcene T., Abdelaziz B., Brahim B., Poly (acrylamide (AM)-co-4-vinylpyridine (4-VP)) quaternized by alkylbromides for removal of chromium (VI), *Mor. J. Chem.* 3 (2015) 122-126.
17. Liu W., Zhang J., Zhang Ch., Wang Y., Li Y., Adsorptive removal of Cr (VI) by Fe-modified activated carbon prepared from Trapa natans husk, *Chem. Eng. J*. 162 (2010) 677-684.

18. Nethaji S., Sivasamy A., Mandal A.B., Preparation and characterization of corn cob activated carbon coated with nano-sized magnetite particles for the removal of Cr(VI), *Bioresource Technol*, 134 (2013) 94-100.
19. Liu H., Liang Sh., Gao J., Ngo H.H., Guo W., Guo Z., Wang J., Li Y., Enhancement of Cr(VI) removal by modifying activated carbon developed from Zizania caduciflora with tartaric acid during phosphoric acid activation, *Chem. Eng. J*. 246 (2014) 168-174.
20. Zhao Y., Zhao D., Chen Ch., Wang X., Enhanced photo-reduction and removal of Cr(VI) on reduced graphene oxide decorated with TiO_2 nanoparticles, *J. Colloid Interface Sci*. 405 (2013) 211-217.
21. Hao T., Yang Ch., Rao X., Wang J., Niu Ch., Su X., Facile additive-free synthesis of iron oxide nanoparticles for efficient adsorptive removal of Congo red and Cr(VI), *Applied Surface Sci*. 92 (2014) 174-180.
22. Yao W., Ni T., Chen Sh., Li H., Lu Y., Graphene/Fe_3O_4 and polypyrrole nanocomposites as a synergistic adsorbent for Cr(VI) ion removal, *Composites. Sci Technol*. 99 (2014) 15-22.
23. Sun X., Yang L., Li Q., Zhao J., Li X., Wang X., Liu H., Amino-functionalized magnetic cellulose nanocomposite as adsorbent for removal of Cr(VI): Synthesis and adsorption studies, *Chem. Eng. J*. 241 (2014) 175-183.
24. Bhaumik M., Setshedi K., Maity A., Onyango M.S., Chromium(VI) removal from water using fixed bed column of polypyrrole/Fe_3O_4 nanocomposite, *Separation. Purif. Technol*. 110 (2013) 11-19.
25. Pan J.j, Jiang J., Xu R.k, Removal of Cr(VI) from aqueous solutions by Na_2SO_3/$FeSO_4$ combined with peanut straw biochar, *Chemosphere*. 101 (2014) 71-76.
26. Ng I.S, Wu X., Yang X., Xie Y., Lu Y., Chen C., Synergistic effect of Trichoderma reesei cellulases on agricultural tea waste for adsorption of heavy metal Cr(VI) *Bioresource Technol*. 145 (2013) 297-301.
27. Li T., Shen J., Huang Sh., Li N., Ye M., Hydrothermal carbonization synthesis of a novel montmorillonite supported carbon nanosphere adsorbent for removal of Cr (VI) from waste water, *Applied. Clay. Sci*. 93-94 (2014) 48-55.
28. Wang W., Zhou J., Achari G., Yu J., Cai W., Cr(VI) removal from aqueous solutions by hydrothermal synthetic layered double hydroxides: Adsorption performance, coexisting anions and regeneration studies, *Colloids Surfaces A: Physicochem. Eng. Aspects*. 457 (2014) 33-40.
29. Ansari R., Fahim N.K., Application of polypyrrole coated on wood sawdust for removal of Cr(VI) ion from aqueous solutions, *React. Funct. Polym.* 67 (2007) 367-374.
30. Ansari R., Pornahad A., Removal of Ce(IV) Ions from aqueous solutions using sawdust coated by electroactive polymers, *Sep. Sci. Technol.* 45 (2010) 2376-2382.
31. Ansari R., Seyghali B., Mohammad-khah A.; Zanjanchi M.A., Application of nano surfactant modified Biosorbent as an efficient adsorbent for dye removal, *Sep. Sci. Technol*. 47 (2012) 1802-1812.
32. Suresh G., Babu B.V., Modeling, simulation, and experimental validation for continuous Cr(VI) removal from aqueous solutions using sawdust as an adsorbent, *Bioresour. Technol.* 100 (2009) 5633-5640.
33. Anees A., Mohd R., Othman S., Mahamad H.I., Yap Y.C., Bazlul M.S., Removal of Cu(II) and Pb(II) ions from aqueous solutions by adsorption on sawdust of Meranti wood, *Desalination*. 247 (2009) 636-646.
34. Eaton A.D., Clesceri L.S., Greenberg A.E., Standard Methods for the Examination of Water and Wastewater, 19th ed., American Public Health Association American Water Works Association and Water Environment Federation, Washington, DC, 1995.
35. Sullivan K.T., Wu Ch., Piekiel N.W., Gaskell K., Zachariah M.R., Synthesis and reactivity of nano-Ag_2O as an oxidizer for energetic systems yielding antimicrobial products, *Combustion and Flame*. 160 (2013) 438-446.
36. Gilcreas F.W., Tarars M.J., Ingols R.S., Standard Methods for the Examination of Water and Wastewater, 12th ed, American Public Health Association (APHA) Inc., New York, 1995.
37. Ballav N., Maity A., Mishra S. B., High efficient removal of chromium (VI) using glycine doped polypyrrole adsorbent from aqueous solution, *Chem. Eng. J*. 198-199 (2012) 536-546.

38. Bhaumik M., Maity A., Srinivasu V.V., Onyango M. S., Removal of hexavalent chromium from aqueous solution using polypyrrole-polyaniline nanofibers, *Chem. Eng. J*. 181-182 (2012) 323-333.
39. Yang J., Qi L., Zhang D., Ma J., Cheng H., Dextran-Controlled Crystallization of Silver Microcrystals with Novel Morphologies, *Crystal Growth & Design*. 4 (2004) 6.
40. Janardhanan R., Karuppaiah M., Hebalkar N., Rao T.N., Synthesis and surface chemistry of nano silver particles, *Polyhedron*. 28 (2009) 2522-2530.
41. Gode F., Atalay E.D., Pehlivan E., Removal of Cr(VI) from aqueous solutions using modified red pine sawdust, *J. Hazard. Mater*. 152 (2008) 1201-1207.
42. Rahman M.M., Khana Sh.B., Asiri A.M., Al-Sehemi A.G., Chemical sensor development based on polycrystalline gold electrode embedded low-dimensional Ag_2O nanoparticles, *Electrochimica Acta*. 112 (2013) 422-430.
43. Deng Sh., Bai Re., Removal of trivalent and hexavalent chromium with aminated polyacrylonitrile fibers: performance and mechanisms, *Water. Res*. 38 (2004) 2424-2432.
44. Kyzas G.Z., Kostoglou M., Lazaridis N.K., Copper and Cr(VI) removal by chitosan derivatives-Equilibrium and kinetic studies, *Chem. Eng. J*. 152 (2009) 440-448.
45. Monahar D.M., Anoop K.K., Anirudhan T.S., Removal of mercury(II) from aqueous solutions and chlor-alkali industry wastewater using 2-mercaptobenzimidazole-clay. *Water. Res*. 36 (2002) 1609-1619.
46. Dawodu F.A., Akpomie K.G., Simultaneous adsorption of Ni(II) and Mn(II) ions from aqueous solution unto a Nigerian kaolinite clay, *J. Mater. Res. Technol*. 3(2014) 129-141.
47. Vaghetti J. C.P., Limaa E.C., Royera B., Brasil J. L., da-Cunha B. M., Simona N. M., Cardoso N.F., Norena C. P. Z., Application of Brazilian-pine fruit coat as a biosorbent to removal of Cr(VI) from aqueous solution—Kinetics and equilibrium study, *Biochem. Eng. J*. 42 (2008) 67-76.
48. Tempkin M. J., Pyzhev V., Recent modifications to Langmuir isotherms, *Acta. Physiochem. URSS*. 12 (1940) 217-222.
49. Saroj S. S., Surendra N. D., Pradip R., Hexavalent chromium removal from aqueous solution by adsorption on treated sawdust, *Biochem. Eng. J*. 31 (2006) 216-222.
50. Fethiye G., Elif D. A., Erol P., Removal of Cr(VI) from aqueous solutions using modified red pine sawdust, *J. Hazard. Mater*. 152 (2008) 1201–1207.
51. Alaerts G.J., Jitjaturant V., Kelderman P., Use of coconut shell based activated carbon for chromium (VI) removal, *Water Sci. Technol*. 21 (1989) 1701–1704.